

**Inferring LTI Dynamics of Inverter Based Resources in
Isolated and Networked Scenarios**

**A THESIS
SUBMITTED TO THE FACULTY OF THE GRADUATE SCHOOL
OF THE UNIVERSITY OF MINNESOTA
BY**

Samuel Helman

**IN PARTIAL FULFILLMENT OF THE REQUIREMENTS
FOR THE DEGREE OF
MASTER OF SCIENCE**

Sairaj Dhople

May, 2024

Acknowledgements

My deepest thanks to:

Professor Sairaj Dhople, who has been a fantastic and generous mentor and PI during this thesis and my master's degree in general.

Hyeonjung(Tari) Jung and Professor Manish Singh, whose knowledge has been invaluable in guiding me through the complexities of power systems and control theory.

Dr. Nathan Baeckeland, who built the original GFM models used in this thesis and patiently explained their inner workings to me.

Professors Murti Salapaka and Eric Severson, for their time and feedback in reviewing this thesis.

And of course my wife Anna, whose support makes everything possible.

Abstract

This thesis demonstrates multiple methods for simplifying and understanding the nonlinear power dynamics of grid-forming inverters (GFMs) and aggregating those dynamics into larger networks. First, a model of a GFM as a current-controlled voltage source is examined. The nonlinear power dynamics are analytically linearized and the behavior is compared to the original nonlinear model. Second, the power and frequency outputs of a more complex GFM model are fed into system identification software in order to fit them to a predetermined linear time-invariant (LTI) system and learn system parameters such as inertia and droop. For comparison, the same system identification techniques are then applied to the outputs of a simplified synchronous generator model. Finally, a modified IEEE 14-bus network configuration including five GFMs and three variable loads is simulated, and the resulting power and frequency dynamics are fit to the same LTI system. The intent is threefold: first, to demonstrate the appropriateness of LTI models in describing the power dynamics of individual GFMs and synchronous generators, in order to facilitate analysis of larger networked systems; second, to discover the relationship between internal control parameters of GFMs and their externally observed values; and third, to validate that grey-box data-driven system identification techniques can be a valuable tool for discovering the values of important parameters in the absence of explicit vendor models.

Contents

Acknowledgements	i
Abstract	ii
List of Tables	v
List of Figures	vi
1 Introduction	1
2 Power Dynamics of a Current-Controlled Voltage Source	4
2.1 Description of Equivalent Circuit Model	4
2.2 Nonlinear Power Dynamics	5
2.3 Linearization of Power Dynamics	6
2.4 Simulation Validation	7
3 Power Dynamics of Grid-Forming Inverters	9
3.1 Original High-Order GFM Models	9
3.2 Reduced-Order Model for Power and Frequency Dynamics	11
3.3 System Identification	11
3.4 Simulation Validation	13
4 Power Dynamics of Simplified Synchronous Generators	16
4.1 Description of Synchronous Generator Model	16
4.2 Simulation Validation	18

5	Power Dynamics of Networked Grid-Forming Inverters	19
5.1	Description of LTI Dynamics	19
5.2	Description of High-Order Simulation	20
5.3	Simulation Validation	22
6	Conclusion and Discussion	25
	References	27
	Appendix A. Glossary and Acronyms	29
A.1	Glossary	29
A.2	Acronyms	30

List of Tables

2.1	Parameter values for the C CVS simulation cases	7
3.1	Specified vs. learned parameter values for the simulation of the nonlinear GFM model	15
4.1	Specified vs. learned parameters for the simulation of a single synchronous generator	18
5.1	AGC parameters for the simulation of networked GFMs	21
5.2	Cost functions and control schemes for the simulation of networked GFMs	22
5.3	Specified vs. learned parameters for the simulation of networked GFMs	24
A.1	List of acronyms	30

List of Figures

2.1	CCVS equivalent circuit	5
2.2	Comparison of original vs. linearized CCVS dynamics	8
3.1	Internal architecture of the nonlinear GFM model	10
3.2	Overview of the system identification process	12
3.3	Results of the system identification process for the nonlinear GFM model: Case 1	14
3.4	Results of the system identification process for the nonlinear GFM model: Case 2	14
4.1	Results of the system identification process for a single synchronous gen- erator	17
5.1	Diagram of the IEEE 14-bus network	20
5.2	Results of the system identification process for the IEEE 14-bus network	22

Chapter 1

Introduction

The power grid is in the process of transitioning to a greater reliance on distributed inverter-based resources (IBRs), such as solar photovoltaics and battery-based storage systems. With this transition comes the need for accurate and scalable mathematical models of how these resources behave, both in isolation and as part of a larger network [1]. There are two principal categories of IBRs: grid-following (GFL) and grid-forming (GFM) IBRs. GFLs synchronize to the external frequency provided by the grid, following the lead of the resources to which they are connected. GFMs, on the other hand, implement internal controls that set the frequency at their terminals, and therefore contribute to maintaining the external frequency of the grid. Because of this ability, GFMs are a key piece of replacing traditional spinning generators for stabilizing the grid under both normal and abnormal conditions [2], [3]. However, GFMs are built by a wide array of vendors and manufacturers, who are apprehensive to reveal the internal parameters - such as inertia and droop - of their machines. Therefore, data-driven modeling that can take the outputs of existing GFMs and use them to learn the parameters and behavior of the internal systems is a valuable tool for researchers.

System identification, which we explore in this thesis, is an umbrella term for a suite of mathematical techniques that attempt to discover the dynamics of an underlying system based on the system's observed response to a set of inputs. In particular, the usefulness of grey-box modeling in understanding the observed behavior of power systems is gaining traction with researchers [4], [5], [6]. Grey-box modeling combines many of the positive features of physics-based white-box modeling and data-driven black-box

modeling. White-box models attempt to simulate the entire internal dynamics of a well-understood system; black-box models, on the other hand, treat the system internals as entirely opaque and draw conclusions based solely on the outputs. Grey-box modeling uses the outputs of the system, combined with some a priori knowledge of the parameters and structure of the internals, to discover a set of dynamics that fits well to the outputs [7]. This can be an excellent fit for IBRs, whose internal dynamics are studied but whose vendor-specific parameters and externally observed behavior are not always known. For the examples in this thesis, system identification can be thought of as a form of curve-fitting of linear to nonlinear dynamics.

Substantial literature exists and continues to be developed on primary GFM controls: how to design the internals of the system in order to achieve the desired power and frequency performance at the terminals [8], [9], [10]. Additionally, optimization and behavior of traditional secondary and tertiary control is well-studied both throughout history [11] and actively in the current day [12], [13]. However, as GFMs become more prevalent, a greater understanding of secondary and tertiary control in systems with high GFM penetration is needed, as well as the applicability of traditional results to these systems. In order for this to be accomplished, it is necessary to develop mathematical models of GFMs that are both accurate and scalable, and can be combined with models of traditional synchronous generators in a unified system. These models must faithfully represent the behavior of individual GFMs, but be able to be aggregated without an explosion of complexity in order to facilitate analytical results.

This thesis describes two main contributions. The first is a set of methods for simulating nonlinear and high-order GFM models and then comparing how closely their behavior fits to simpler linear time-invariant (LTI) systems. In particular, we use modern system identification techniques in order to compare the systems where analytical work is infeasible due to complexity. This is done in order to verify that the LTI model in question are usable for larger-scale analysis, mitigating the explosion of complexity discussed above. The second contribution is in using the same system identification methods to determine important parameters, such as inertia and droop, of the nonlinear and high-order models. This helps determine whether the external values can be mapped directly to tunable parameters in the models, and thus discovered via inspection in the future.

The organization of this thesis is as follows:

- Chapter 2 presents the results from fitting the outputs of a controlled voltage source model of a GFM with nonlinear power dynamics to a linearized version of the same system. This is done in order to show the applicability of linear dynamics to the modeling of IBRs, and to motivate the more complex examples in further chapters.
- Chapter 3 simulates complex models of individual GFMs based on prior literature [14] and compares the results to the simpler LTI model proposed in [15]. This is done using system identification techniques. In order to provide the necessary context, an overview of the specifics of these techniques and the system identification software used is presented.
- Chapter 4 extends the system identification process to a high-order synchronous generator model in order to demonstrate the applicability of the LTI model to heterogenous generating resources.
- Chapter 5 extends the results from chapter 3 to a networked group of high-order GFMs. The LTI model is enhanced to include the results of secondary and tertiary control, and the simulation results are fit to the updated dynamics using the same system identification techniques as in chapter 3.
- Chapter 6 draws conclusions and presents directions for future work.

Chapter 2

Power Dynamics of a Current-Controlled Voltage Source

This section considers a simplified equivalent-circuit model for an IBR as a current-controlled voltage source with nonlinear power dynamics. The dynamics are linearized about a steady-state operating point, and the power dynamics of the resulting LTI system are compared to the original nonlinear model. This is intended to:

1. Demonstrate that linearized power dynamics for simplified IBR models can faithfully represent the original nonlinear dynamics.
2. Motivate the use of system identification techniques to find LTI parameters for the more complex examples in the following chapters, where the nonlinear power dynamics are highly difficult to analytically linearize.

2.1 Description of Equivalent Circuit Model

To illustrate the challenges in capturing the dynamics of power injections from controlled sources and the potential of linear models in describing the same, we consider the current-controlled voltage source (CCVS) connected to an infinite bus through an

inductive transmission line illustrated in Fig. 2.1. This model is adopted from [16].

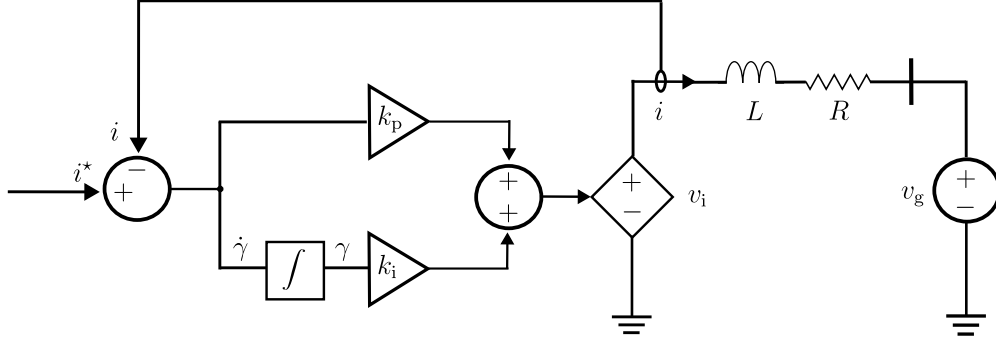


Figure 2.1: Equivalent circuit diagram of the CCVS with nonlinear power dynamics.

The CCVS dynamics are governed by a proportional-integral (PI) controller that modulates current injection to track a desired reference. The system is characterized by two states: the current, i , and an internal control state, γ . The dynamics of the system are given by

$$L \frac{di}{dt} = k_p(i^* - i) + k_i \gamma - v_g - iR, \quad (2.1)$$

$$\frac{d\gamma}{dt} = i^* - i, \quad (2.2)$$

where i^* is the current setpoint; v_g is the infinite-bus voltage; L and R are the inductance and resistance of the line between the source and load; and k_p and k_i are the proportional and integral gains of the PI controller. In what follows, we consider i^* and v_g to be the two exogenous inputs to the system. By construction, the voltage at the terminals of the CCVS, v_i , is given by

$$v_i = k_p(i^* - i) + k_i \gamma. \quad (2.3)$$

2.2 Nonlinear Power Dynamics

Utilizing the expression for v_i from (2.3), we obtain the following expression for the instantaneous power delivered by the CCVS

$$p = v_i i = (k_p(i^* - i) + k_i \gamma) i. \quad (2.4)$$

To extract the power dynamics for the C CVS above, we take the time-based derivative of the instantaneous power injection p . This yields:

$$\begin{aligned}\frac{dp}{dt} &= \frac{d}{dt} v_i i = \frac{d}{dt} \frac{k_p i^* i - k_p i^2 + k_i \gamma i}{L} \\ &= \frac{k_p i^*}{L} \frac{di}{dt} - \frac{2k_p i}{L} \frac{di}{dt} + \frac{k_i \gamma}{L} \frac{di}{dt} + \frac{k_i i}{L} \frac{d\gamma}{dt}.\end{aligned}$$

Substituting for dynamics of i and γ from (2.1) and (2.2), leveraging the definition for p from (2.4) and $p = i^2 R + i v_g$ (based on power balance in the equivalent circuit Fig. 2.1), we arrive at

$$\begin{aligned}\frac{dp}{dt} &= \frac{-k_p - R}{L} p + \frac{-k_p^2 i^* + k_p v_g + L k_i i^*}{L} i \\ &\quad + \frac{2k_p k_i i^* - k_i v_g \gamma - \frac{k_p k_i}{L} i \gamma + \frac{(k_i \gamma)^2}{L}}{L} - k_i i^2 \\ &\quad + \frac{(k_p i^*)^2}{L} - \frac{k_p i^* v_g}{L}.\end{aligned}\tag{2.5}$$

Notice that the above dynamics are nonlinear in states and inputs. This severely challenges analysis.

2.3 Linearization of Power Dynamics

Next, we linearize the dynamics above about a steady-state operating point in order to compare the behavior of the resulting LTI model to the original nonlinear system. Denote $\Delta p = p - \bar{p}$, $\Delta i = i - \bar{i}$, $\Delta \gamma = \gamma - \bar{\gamma}$, where \bar{p} , \bar{i} , and $\bar{\gamma}$ are equilibrium values of the power, current, and control state variables given by

$$\bar{p} = \bar{i}^* \bar{v}_i = \bar{i}^{*2} R + \bar{i}^* \bar{v}_g, \quad \bar{i} = \bar{i}^*, \quad \bar{\gamma} = \frac{1}{k_i} \bar{v}_g + \frac{R}{k_i} \bar{i}^*.\tag{2.6}$$

Above, \bar{i}^* and \bar{v}_g are the values of the system inputs that correspond to the steady-state values used for the linearization. Changes to the inputs around the values that define steady-state operation are denoted $\Delta i^* = i^* - \bar{i}^*$ and $\Delta v_g = v_g - \bar{v}_g$. Dynamics of $\Delta \dot{p}$, $\Delta \dot{i}$, and $\Delta \dot{\gamma}$ can be expressed as:

$$\begin{bmatrix} \Delta \dot{p} \\ \Delta \dot{i} \\ \Delta \dot{\gamma} \end{bmatrix} = A \begin{bmatrix} \Delta p \\ \Delta i \\ \Delta \gamma \end{bmatrix} + B \begin{bmatrix} \Delta i^* \\ \Delta v_g \end{bmatrix},\tag{2.7}$$

$$A = \begin{bmatrix} \frac{-k_p - R}{L} & \frac{-k_p^2 \bar{i}^* + k_p \bar{v}_g + L k_i \bar{i}^* - k_p k_i \bar{\gamma} - 2L k_i \bar{i}}{L} & \frac{2k_p k_i \bar{i}^* - k_i \bar{v}_g - k_p k_i \bar{i} + 2k_i^2 \bar{\gamma}}{L} \\ 0 & \frac{(-k_p - R)}{L} & \frac{k_i}{L} \\ 0 & -1 & 0 \end{bmatrix}, \quad B = \begin{bmatrix} \frac{k_p}{L} & \frac{-1}{L} \\ 0 & \frac{k_p}{L} \\ 0 & 1 \end{bmatrix}. \quad (2.8)$$

where Jacobian matrices A, B can be obtained from the originating dynamics (2.1), (2.2), and (2.5). The full Jacobian expansion is given in (2.8).

2.4 Simulation Validation

To compare the originating nonlinear power dynamics with the LTI approximation, we simulate three separate cases for each system in order to understand how varying the relationship of the control parameters k_i and k_p affects behavior. The non-control parameters are kept constant. The cases are given in the table below. For mathematical convenience, we pick $\bar{i}^* = \bar{v}_g = 1$ as the operating point for linearization. All systems begin at steady-state, and respond to an immediate step change of $\Delta i^* = 0.2$, $\Delta v_g = 0.2$.

	L (H, p.u.)	R (Ω , p.u.)	k_i (F^{-1} , p.u.)	k_p (Ω , p.u.)
Case 1	1	0.1	1	1
Case 2	1	0.1	1	0.5
Case 3	1	0.1	1	2

Table 2.1: Parameter values for the different cases run for the nonlinear vs. linearized CCVS model.

Figure 2.2 shows the results of the two cases described above for both the nonlinear system from section 2.2 and the linearized model from section 2.3. Since the original dynamics (2.1) for i and (2.2) γ are linear, the i and γ outputs of the linearized system can be seen to exactly track the values from the nonlinear system. The power dynamics settle to within a steady-state error of 0.05 per-unit in all three cases, with the error in the transient response affected by the control parameters: a lower ratio of proportional gain to integral gain produces a larger transient error.

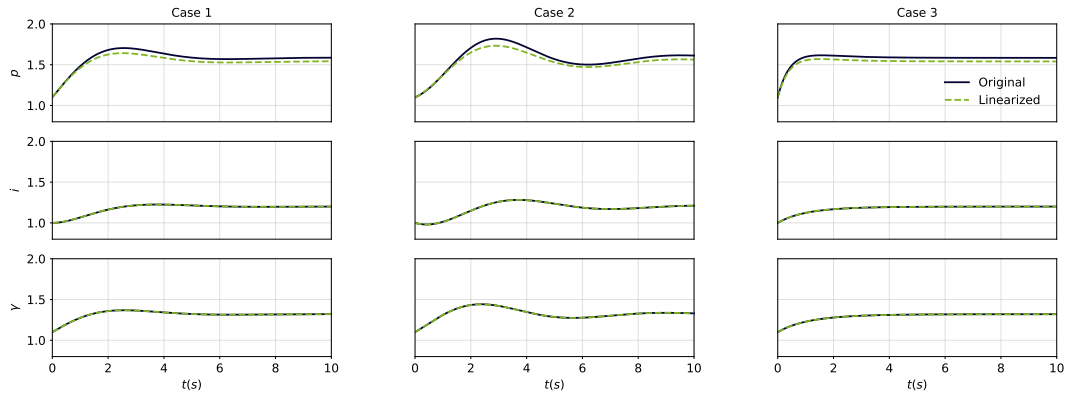


Figure 2.2: Responses of the original nonlinear system vs. the linearized system for the CCVS model.

The results from this example help illustrate that linearization of power dynamics for simplified IBR models is a fruitful avenue to pursue. This helps to motivate the system identification techniques applied in the second half of this paper. The GFM models that we will see in the following section are too complex to be analytically linearized, and a combination of engineering judgement and software-based system identification must be used in order to build a linearized model that we can fit to the original.

Chapter 3

Power Dynamics of Grid-Forming Inverters

In this chapter, we attempt to uncover the output-power dynamics of grid-forming IBRs with different primary control types using structured system identification as a tool. The intent is to show that in cases where analytical linearization is infeasible or an involved undertaking due to the complexity of the originating nonlinear models, system identification of a structured linear representation can sufficiently well describe output-power dynamics. While so doing, we compare the parameters of the learned models (focusing on key parameters of inertia constants, damping constants, and droop gains) to the values learned by system identification of the model outputs in order to understand how closely the system identification process preserves the important parameters of the original system.

3.1 Original High-Order GFM Models

For our originating nonlinear GFM models, we use the representation of the internals of a GFM as described in [14]. The GFM internals, broad architecture of which is sketched in Fig. 3.1, include a primary-control unit that regulates the frequency and voltage amplitude of the IBR. Three different primary-control strategies are examined: droop control, dispatchable virtual oscillator (dVOC) control, and virtual synchronous machine (VSM) control. The remainder of the control architecture includes voltage

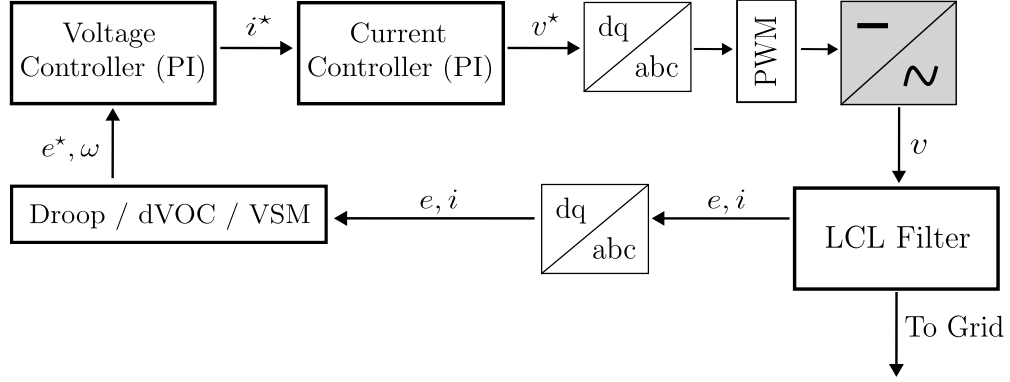


Figure 3.1: Internal architecture of the high-order GFM model. e and e^* represent actual and setpoint values for internally-measured voltage.

control, current control, an output *LCL* filter, and current limiting. For modeling larger networks, the dynamics of the power output at the terminals of the GFM is important in understanding how it will respond to changes in load. However, because of the extra components connected to the control unit, the terminal power dynamics are high-order and nonlinear, and describing their dynamics accurately based on the whole internal system is often infeasible. This means that the linearization procedure from Section 2.3 can be highly difficult to pursue. Instead, we use system identification techniques to learn an LTI system that closely approximates the dynamics of power outputs of the full-order GFM model.

GFM models for the three different control strategies (droop, dVOC, and VSM) were implemented in Simulink using components from the Specialized Power Systems (SPS) Toolbox. The three models all use the internal architecture shown in Fig. 3.1, and are identical other than the specifics of the internal frequency control unit. The outputs of the models are the power injections into the grid, as well as the frequency of the voltage measured at the terminals of the GFM. All simulations are run in a balanced three-phase environment.

3.2 Reduced-Order Model for Power and Frequency Dynamics

We now introduce an LTI model intended to capture the power and frequency dynamics of GFM inverters. The model is inspired by the swing equations of synchronous generators and was postulated in [15]. The aptness of this model to capture the power dynamics of GFM inverters will be investigated in this effort. The dynamics of the LTI model are

$$M\Delta\dot{\omega} = -D\Delta\omega + p - d, \quad (3.1a)$$

$$\tau\dot{p} = p^* - p + R\Delta\omega, \quad (3.1b)$$

where $\Delta\omega$ is the deviation in terminal frequency from nominal, p captures the output power of the GFM IBR, M and D denote inertia and damping factors, d is the demand that the resource is serving, τ captures the power-adjustment time constant, R is the (equivalent, in the case of dVOC) droop coefficient, and p^* is the power reference provided by a higher-level hierarchical controller (e.g., automatic generation control (AGC)). In order for the equations to be consistent, the units of the inertia factor M are defined as $\text{s}^2 * \text{rad}^{-1}$, and the units of both D and R are $\text{s} * \text{rad}^{-1}$.

This set of equations is intended as a generalized version of the classical swing and primary control equations that are well-studied as behavioral models for synchronous generators. We choose these equations for our LTI model in order to move towards their applicability to model power outputs of groups of heterogenous resources: if they fit well to the outputs of individual GFM resources, then with an adjustment of parameters they should be usable for grids including both GFMs and classical synchronous generators. That said, in this effort, we focus primarily on validating this model via system identification against the originating higher-order GFM IBR models.

3.3 System Identification

The specific implementation of system identification that we use for this paper is the System Identification Toolbox (SIT) within Matlab. The SIT has grey-box modeling built in as one of the principal features, and allows the user to pick the structure of the

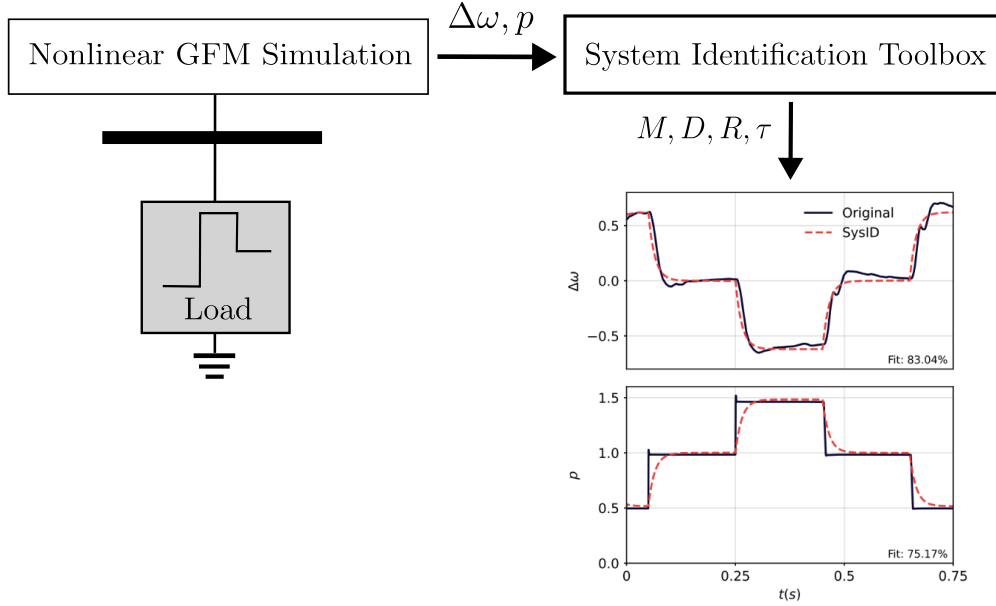


Figure 3.2: Flow of the system identification process. Outputs from the nonlinear simulation are fed into the SIT in order to learn parameters for the specified LTI system.

state-space matrices as well as the parameters that the toolbox will learn. By default, the SIT tunes the parameters of the identified model using a regression fit between the observed outputs and those of the LTI model, with a weighted sum-of-squares error as the loss function [17]. For our purposes, we were able to achieve the desired results using the default settings of the SIT. In order to avoid an explosion of complexity in the possible permutations of settings, we therefore left them as the defaults, and will explicitly call out any changes to defaults when discussing the specific results.

The process we use in this paper for system identification using the SIT is as follows:

1. Simulate the original nonlinear system using Simulink, saving frequency and power outputs for the GFM to the workspace.
2. Construct an `idgrey` object in Matlab that specifies the structure of the simplified LTI state-space matrices as well as which parameters are fixed vs. learnable (see [17] as well as the SIT online documentation for full details and examples).
3. Run the `greyest` Matlab function to fit the `idgrey` LTI model to the outputs of the simulation. The SIT performs the regression fit described above to determine

the values of system parameters that provide the closest match between the LTI outputs and those of the original nonlinear system.

4. Simulate the learned LTI system and plot the outputs alongside those of the original nonlinear system.
5. Compare the learned parameter values for the LTI system to corresponding parameters of the nonlinear models.

The comparison between the outputs of the original and learned systems for the given inputs is accomplished via the `compare` function in Matlab, which performs a normalized root mean square comparison [17] and returns the quality of the fit as a percentage value, with 100% as a perfect fit.

3.4 Simulation Validation

Two different cases were simulated for the high-order GFM models described in Section 3.1. In both cases, an individual GFM was connected to the three-phase load model included in the SPS toolbox. The load was then programmed to vary by multiple step changes, and the GFM's frequency offset from nominal as well as power injection were recorded. All internal parameters of the GFMs were kept constant.

The first case consists of a series of step changes in load up and back down, in a ziggurat pattern. The second case consists of a step up, followed by a large step down below the original load before returning to the baseline. The outputs of the higher-order models were fit to the LTI system from Section 3.2, with M , D , R , and τ as learnable parameters.

System identification results for the first case are shown in Fig. 3.3, and results for the second case are shown in Fig. 3.4: $\Delta\omega$ is the difference between nominal frequency (60 hz) and the frequency as measured at the GFM's terminals, multiplied by a factor of 2π to represent angular frequency. p is the output power of the GFM in per-unit. The fit percentage is the normalized root mean square comparison as reported by the SIT.

It can be readily seen from Fig. 3.3 and Fig. 3.4 that for all three control types, the LTI system provides a close approximation to the behavior of the original nonlinear

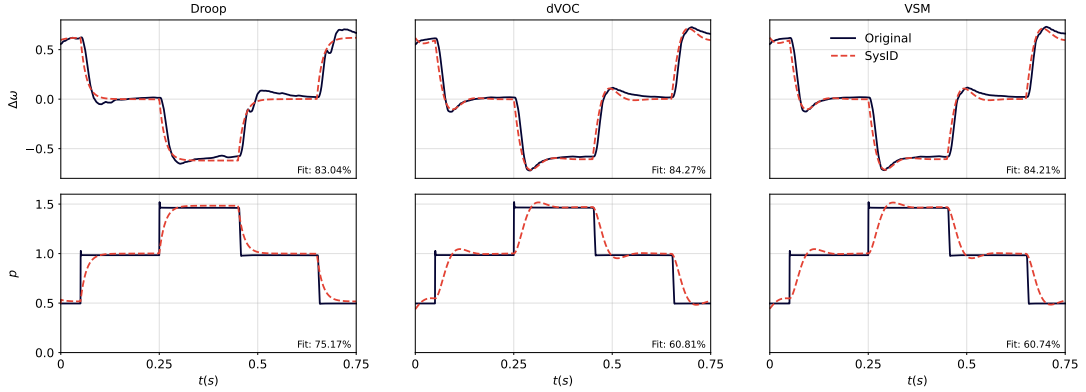


Figure 3.3: Case 1 results of fitting the high-order simulation outputs to the LTI model.

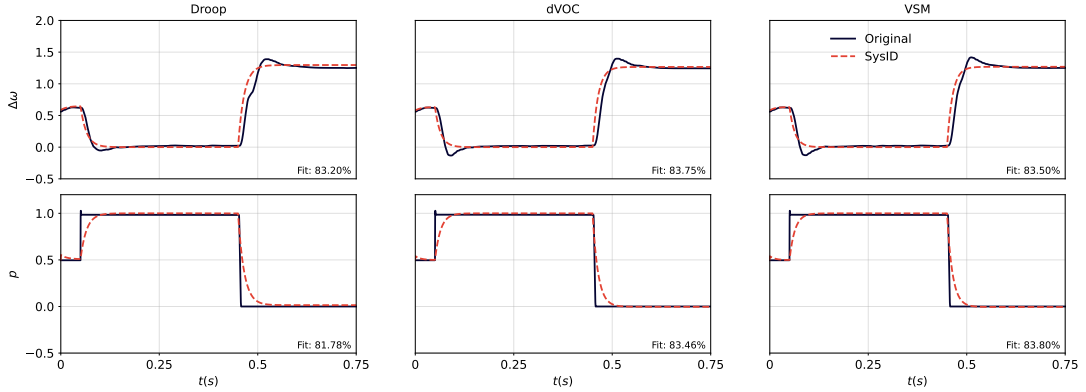


Figure 3.4: Case 2 results of fitting the high-order simulation outputs to the LTI model.

dynamics. In five of the six simulations, the frequency offset is a closer fit than the power dynamics; in particular, the rise time in power is slower for the learned LTI system than the original model. The overall result—that the LTI dynamics can be a close match for the behavior of individual GFM resources—is an important building block in future efforts to fit the model to larger, multi-resource, and heterogenous systems.

We next compare the parameters specified in the nonlinear simulations to the learned parameters for the LTI system. The high-order droop control unit accepts a droop parameter, and the VSM control unit accepts parameters for inertia, damping, and droop. In the following table, we show how accurately these parameters correspond to the values learned by the SIT for the M , D , and R LTI parameters. The values of the parameters specified for the high-order simulations are listed as $\text{inertia}_{\text{sim}}$, $\text{damping}_{\text{sim}}$,

and $\text{droop}_{\text{sim}}$. The M_{VSM} notation represents the value of M learned by the SIT from the outputs of the simulation of the VSM-based GFM.

Based on these results, the inertia parameter in the high-order VSM model appears to be a close predictor of the M parameter when fitted to the LTI model. Additionally, the droop parameter stays very close to the learned R value for both the VSM and droop control units. Both of these are promising results: because the learned parameters of the LTI system match closely to the corresponding parameters in the high-order models, it is easier to tune these values in the high-order models with confidence as to the resulting behavior. The learned D value for VSM control varies widely between the two cases and does not closely match the damping input for the high-order VSM model; more work is needed to determine if any appropriate mapping can be made.

	Case 1	Case 2
$\text{inertia}_{\text{sim}}$	0.0106	0.0106
M_{VSM}	0.0151	0.0108
$\text{damping}_{\text{sim}}$	0.0050	0.0050
D_{VSM}	0.0515	-0.0042
$\text{droop}_{\text{sim}}$	-0.8000	-0.8000
R_{droop}	-0.7798	-0.7604
R_{VSM}	-0.7737	-0.7926

Table 3.1: Specified versus learned parameter values for the high-order GFM system identification process.

Chapter 4

Power Dynamics of Simplified Synchronous Generators

In this chapter, we extend the results for individual GFMs from chapter 3 by applying the same system identification process to the outputs of a nonlinear model of a synchronous generator. The intent is to demonstrate that the LTI dynamics presented in (3.1) are applicable for classical synchronous generators in addition to GFMs. This is an important step in using the LTI dynamics to model heterogeneous groups of resources, in order to faithfully describe modern power grids.

4.1 Description of Synchronous Generator Model

The synchronous generator model used for the simulation in this section is the three-phase Simplified Synchronous Machine (SSM) Matlab model from the Simscape toolbox. The model's mechanical internals are partially described by

$$\Delta\omega(t) = \frac{1}{2H} \int_0^t (T_m - T_e) - K_d \Delta\omega(t) dt, \quad (4.1a)$$

$$\omega(t) = \Delta\omega(t) + \omega_0, \quad (4.1b)$$

where H is the constant of inertia, T_m and T_e are the mechanical and electrical torque, and K_d is an internal damping factor. The model accepts a mechanical power reference p_m and voltage setpoint e^* as inputs, and modulates its internal controls to provide the

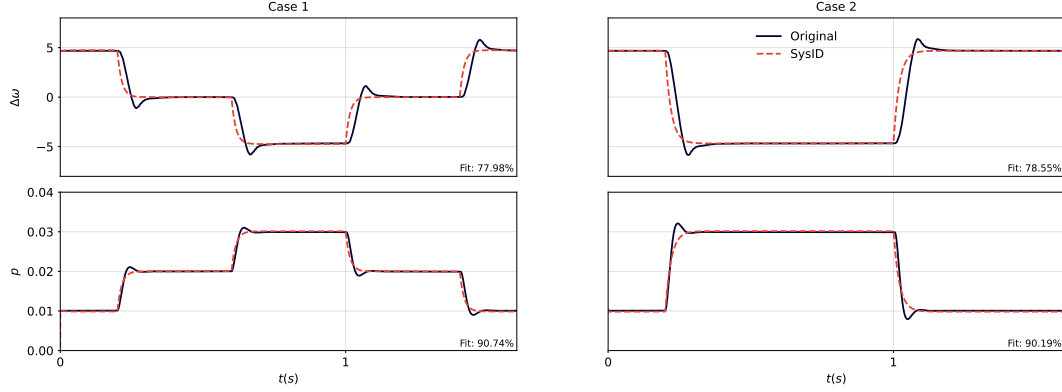


Figure 4.1: Results of fitting the high-order synchronous generator outputs to the LTI model.

desired power. The outputs of the model are the electrical power provided as well as the frequency at the terminals. Note that (4.1) is not a full description of the internals of the SSM block, since other factors such as internal controls and the effects of internal resistance and inductance are not exposed.

In order to match the dynamics from (3.1), we used Simulink to implement primary control on top of the SSM model provided by Matlab. The primary control dynamics implemented are

$$\tau_g p_m = p^* - p_m + R_g \Delta\omega(t), \quad (4.2)$$

with R_g defined as a tunable droop constant. We then hook the SSM, surrounded by primary control, up to two different variable three-phase loads. For consistency, the input variables for inertia, damping, and droop are kept consistent with the $\text{inertia}_{\text{sim}}$, $\text{damping}_{\text{sim}}$, and $\text{droop}_{\text{sim}}$ values from section 3.4. $\text{inertia}_{\text{sim}}$ is adjusted appropriately to be specified as $\frac{1}{2H}$. In addition, the loads closely resemble those in section 3.4. Small changes are made in order to ensure stability of the SSM reaction - notably, both loads start at a non-zero value and vary by only 0.01 per-unit in each step rather than 0.5. Additionally, the simulation time is doubled, in order to allow for transience caused by the unmodeled and unexposed internal dynamics of the SSM.

4.2 Simulation Validation

The results of the SIT process are shown in Fig. 4.1. As can be seen, the LTI dynamics (3.1) that were previously shown to be a good match for high-order GFM outputs are also well-fitted to the synchronous generator model. However, one interesting result comes when we look at the simulated vs. learned parameters, in table 4.1. The learned values are consistent across the two load cases; however, they differ from the provided simulation values by orders of magnitude. This, along with the wide swings in frequency seen in Fig. 4.1, motivates one of the main extensions to this work that will be discussed in the conclusion: simulating heterogeneous networks of GFMs and synchronous generators and applying system identification techniques to the outputs to discover aggregate behavior and parameter values.

	Case 1	Case 2
$\text{inertia}_{\text{sim}}$	0.0106	0.0106
$M_{\text{synch_gen}}$	0.00003085	0.00004399
$\text{damping}_{\text{sim}}$	0.0050	0.0050
$D_{\text{synch_gen}}$	-0.00002742	-0.0000371
$\text{droop}_{\text{sim}}$	-0.8000	-0.8000
$R_{\text{synch_gen}}$	-0.002135	-0.002169

Table 4.1: Specified versus learned parameter values for the high-order synchronous generator system identification.

Chapter 5

Power Dynamics of Networked Grid-Forming Inverters

In this section, we build upon the results from chapter 3 by connecting a networked group of GFMs and variable three-phase loads. We then apply the same system identification techniques as in chapter 3, in order to fit the frequency and power outputs of the network to a simplified set of LTI dynamics.

5.1 Description of LTI Dynamics

The LTI dynamics that we use in this section are an extended version of (3.1), updated to include secondary control of a single area via automatic generation control (AGC) as well as tertiary control via inputs from economic dispatch. The full dynamics, which were postulated in [15], are

$$M\Delta\dot{\omega} = -D\Delta\omega + \mathbf{1}^\top \mathbf{p} - d, \quad (5.1a)$$

$$\tau\dot{\mathbf{p}} = \mathbf{p}^* - \mathbf{p} + \mathbf{R}\Delta\omega, \quad (5.1b)$$

$$\tau_z\dot{z} = -z + \beta\Delta\omega + \mathbf{1}^\top \mathbf{p}, \quad (5.1c)$$

$$\mathbf{p}^* = \mathbf{p}^{\text{ref}} + \mathbf{k}(z - \mathbf{1}^\top \mathbf{p}) \quad (5.1d)$$

where z represents the internal AGC state; τ_z is a time constant that controls the speed of AGC operation; β represents the secondary-control gain; \mathbf{k} collects the AGC

participation factors for each generating resource; and \mathbf{p}^{ref} collects the optimal power setpoints based on economic dispatch. Note that in comparison to (3.1), the power and droop parameters are now vectors with one entry per resource. The frequency parameters, on the other hand, remain scalars, since we examine a single area and make the assumption that frequency within the area is consistent across resources.

5.2 Description of High-Order Simulation

We now describe the details of the simulation whose frequency and power outputs will be fit to the LTI dynamics described in (5.1). The simulation is based on the IEEE 14-bus network, and includes five generating units and three variable loads. The full architecture can be seen in Fig. 5.1.

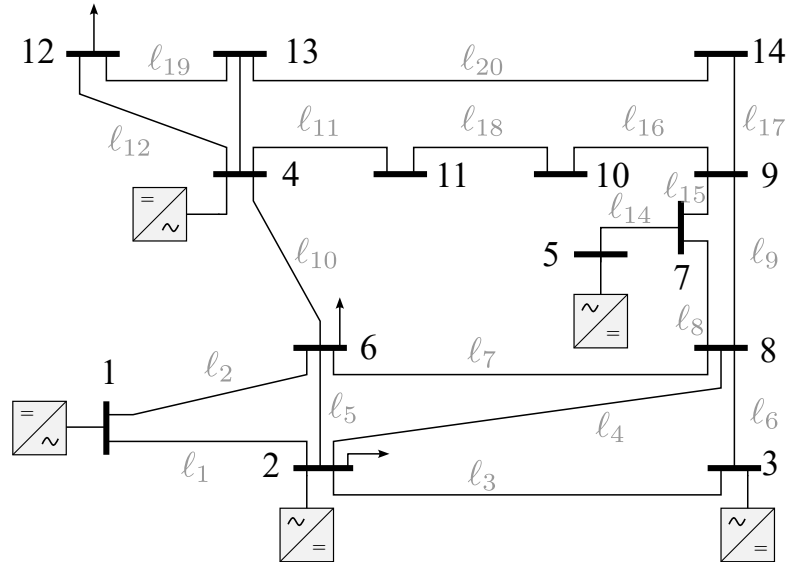


Figure 5.1: 14-bus network used for simulation of collective GFM behavior.

To ensure consistency, each individual GFM is simulated using the same high-order model shown in Fig. 3.1. In order to exercise all control strategies, the GFMs are configured according to table 5.2.

The model postulated in (5.1) does not include line admittances. Therefore, in order to minimize the effect of line parameters on the simulation, all admittances are set to be purely inductive and increased by a factor of 100 from the original 14-bus parameters.

Values for $\text{inertia}_{\text{sim}}$, $\text{damping}_{\text{sim}}$, and $\text{droop}_{\text{sim}}$ are all kept consistent with the values in table 3.1.

The simulation includes AGC implemented via a central controller that provides the power setpoints \mathbf{p}^* to the individual generators. Because the intent of the system identification process is to learn the M , D , and \mathbf{R} parameters and to fit the GFM behavior to the corresponding swing and primary control equations, the dynamics of AGC itself are implemented to match (5.1c) and (5.1d). The values for the tunable parameters are given in table 5.1.

	τ_z	β	\mathbf{k}
Simulation Value	1	-1	$0.2 * \mathbf{1}$

Table 5.1: AGC parameters for the 14-bus network simulation.

The load is varied via a similar zigurat pattern as in Case 1 of section 3.4, with each step change taken by one of the three loads. Economic dispatch is run three times at equal intervals during the simulation in order to provide the \mathbf{p}^{ref} setpoints for AGC, with quadratic cost functions for each resource. The formulation of economic dispatch used is

$$\min_{\mathbf{p}} \sum_g^N C_g(p_g) \text{ s.t.} \tag{5.2a}$$

$$\mathbf{1}^\top \mathbf{p} = d, \tag{5.2b}$$

$$0 \leq p_g \quad \forall g, \tag{5.2c}$$

in which the total cost of generation is minimized subject to meeting demand and keeping power generation non-negative for all resources. The cost functions, which represent cost of generation and are specified per-resource, are shown in table 5.2. The intent with these choices is to be different enough so that power will not be allocated equally by economic dispatch, but close enough such that all generators will be allocated load.

	Control Strategy	Cost Function $C_g(p_g)$
GFM 1	dVOC	$2P_1^2 + P_1 + 4$
GFM 2	droop	$5P_2^2 + P_2 + 3$
GFM 3	VSM	$4P_3^2 + P_3 + 3$
GFM 4	dVOC	$8P_4^2 + P_4 + 2$
GFM 5	droop	$6P_5^2 + P_5 + 5$

Table 5.2: GFM internal control strategies and economic dispatch cost functions for the 14-bus network simulation.

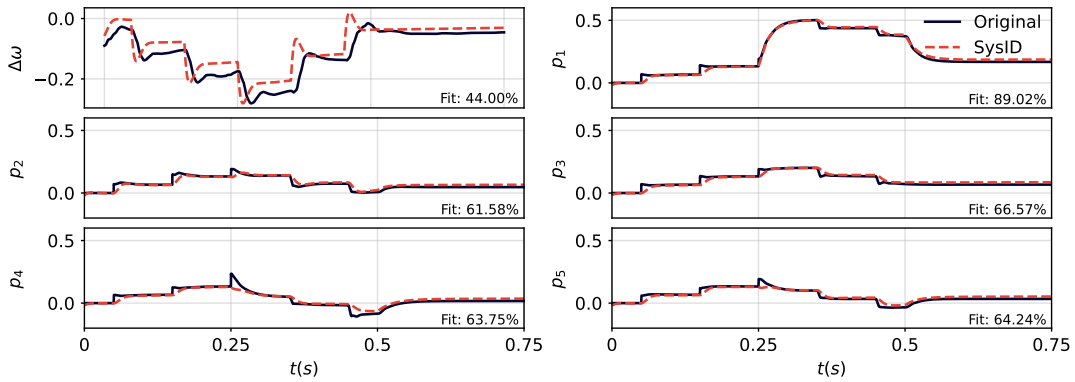


Figure 5.2: Results of fitting the high-order multi-GFM simulation outputs to the LTI model.

5.3 Simulation Validation

The results of the single-area, multi-GFM simulation described above can be seen in Fig. 5.2. As with the previous simulations, $\Delta\omega$ is the difference between nominal frequency (60 Hz) and the frequency as measured at the GFM's terminals, multiplied by a factor of 2π to represent angular frequency. p_i is the output power of GFM $i \in [1, 5]$ in per-unit, and the fit percentage is the normalized root mean square comparison as reported by the SIT.

As in section 3.4, the outputs of the high-order model are compared to the simulated outputs of the learned LTI system, and the percentage fit as reported by the SIT is shown. As seen in the graphs and fit percentages, the LTI power dynamics remain

a strong fit for the higher-order dynamics as in chapter 3, even with the addition of multiple generators, AGC, and economic dispatch. This lends confidence that LTI simplification of power dynamics can be a scalable technique for modeling connected groups of GFMs.

The frequency offset $\Delta\omega$ does not match as closely as the power dynamics, especially during the transience incurred by load and generation changes; the fit quality is only 44%. The steady-state error between the two models at the end of the simulation is 0.015 rad/sec. This does indicate that the differences in behavior of the two models during transience may be mitigated by a small steady-state error once the dynamics settle - more investigation and simulations under different steady-state conditions is needed to verify this.

Table 5.3 shows the provided simulation parameters, as well as the LTI parameters learned by the SIT process. As in section 3.4, the $\text{inertia}_{\text{sim}}$, $\text{damping}_{\text{sim}}$, and $\text{droop}_{\text{sim}}$ are the values provided to the high-order GFM models, which make use of them internally. M and D are the scalar values for M and D learned by the SIT for equation (5.1a), and R_i is the learned value for resource i in the LTI droop vector \mathbf{R} . As before, the learned inertia term M is a relatively close match for the provided inertia, with a difference of 0.0031. The learned droop terms vary more from the provided value of -0.8000 than in the single-GFM simulations, but they are still within 0.2, and notably, the resources' learned droop terms are all close to each other. This lends confidence that overall droop behavior is consistent across resources, and external factors - such as topology, the small but not zero line inductance, and internal resistances - may deviate the learned value from the provided $\text{droop}_{\text{sim}}$.

Consistently with the results of section 3.4, the learned damping factor does not appear to correlate with the value provided to the simulation models. This in itself is an interesting result, and may mean that the damping term is absorbing other dynamics present in the nonlinear dynamics but not explicitly modeled in the LTI system. More investigation is needed to determine what factors affect the final value of this LTI parameter.

	Results
$\text{inertia}_{\text{sim}}$	0.0106
M	0.0075
$\text{damping}_{\text{sim}}$	0.0050
D	2.1270
$\text{droop}_{\text{sim}}$	-0.8000
R_1	-0.6356
R_2	-0.6290
R_3	-0.6397
R_4	-0.6549
R_5	-0.6440

Table 5.3: Specified versus learned parameter values for the high-order multiple-GFM system identification.

Chapter 6

Conclusion and Discussion

In this thesis, we presented methods for simplifying the behavior of nonlinear GFM models down to LTI systems. We compared the power dynamics yielded by both the nonlinear and linearized versions in response to different load changes and with different internal parameters. We then demonstrated that the LTI dynamics are well-fitted to single synchronous generator models, using the same grey-box system identification tools. Finally, we extended the simulation to a group of networked GFM resources with different internal control schemes, in order to show the applicability of the system identification method and learned LTI dynamics to the behavior of multiple resources. The high quality of the fit achieved is intended as a stepping-stone for future work in simulating more complex networks using similar LTI systems.

In addition, we demonstrated a close match between the inertia and droop parameters provided to the high-order models and the corresponding parameters of the LTI system learned by system identification, in the case of a single GFM connected to a load. We compared the provided and learned parameters as well for a group of networked GFMs, showing that the match deviates more from the single resource simulations but remains relatively close. We also showed that the individual learned droop values for the different GFMs are highly consistent with each other.

The clearest path forward into future work is in applying the same system identification techniques using the SIT to networks that include synchronous generators in addition to GFMs. This future work can start with copperplate networks and build towards full models including transmission lines with nontrivial inductances. The work

in this paper helps show that this can be a promising direction. Potential limitations, which need further exploration, include: whether the learned parameters for different configurations of resources will be consistent; whether adding GFLs into the system causes learned parameters or fit to change; and whether specific cases in load patterns or topology will cause the match between original and LTI dynamics to break down. The hope is that the techniques described in this thesis will help future researchers discover simplified LTI dynamics that can be used to model and analyze groups of synchronous generators connected to both GFMs and GFLs. This is therefore a valuable contribution, as simple, accurate, and usable mathematical models that can faithfully represent groups of heterogenous resources are a key piece of understanding and building a decarbonized power grid.

References

- [1] Benjamin Kroposki, Brian Johnson, Yingchen Zhang, Vahan Gevorgian, Paul Denholm, Bri-Mathias Hodge, and Bryan Hannegan. Achieving a 100% renewable grid: Operating electric power systems with extremely high levels of variable renewable energy. *IEEE Power and Energy Magazine*, 15(2):61–73, 2017.
- [2] Yashen Lin, Joseph H. Eto, Brian B. Johnson, Jack D. Flicker, Robert H. Lasseter, Hugo N. Villegas Pico, Gab-Su Seo, Brian J. Pierre, and Abraham Ellis. Research roadmap on grid-forming inverters. 11 2020.
- [3] Florian Dörfler and Dominic Groß. Control of low-inertia power systems. *Annual Review of Control, Robotics, and Autonomous Systems*, 6(Volume 6, 2023):415–445, 2023.
- [4] Junhui Zhang, Yuxi Men, Lizhi Ding, Xiaonan Lu, and Wei Du. Gray-box modeling for distribution systems with inverter-based resources: Integrating physics-based and data-driven approaches. *IEEE Transactions on Industry Applications*, pages 1–9, 2024.
- [5] Yue Zhu, Yunjie Gu, Yitong Li, and Timothy C. Green. Participation analysis in impedance models: The grey-box approach for power system stability. *IEEE Transactions on Power Systems*, 37(1):343–353, 2022.
- [6] Elias Kaufhold, Jan Meyer, and Peter Schegner. Measurement-based identification of dc-link capacitance of single-phase power electronic devices for grey-box modeling. *IEEE Transactions on Power Electronics*, 37(4):4545–4552, 2022.
- [7] L. Ljung. *System Identification: Theory for the User*. Pearson Education, 1998.

- [8] Salvatore D'Arco, Jon Are Suul, and Olav B. Fosso. A virtual synchronous machine implementation for distributed control of power converters in smartgrids. *Electric Power Systems Research*, 122:180–197, 2015.
- [9] M.C. Chandorkar, D.M. Divan, and R. Adapa. Control of parallel connected inverters in standalone ac supply systems. *IEEE Transactions on Industry Applications*, 29(1):136–143, 1993.
- [10] Gab-Su Seo, Marcello Colombino, Irina Subotic, Brian Johnson, Dominic Groß, and Florian Dörfler. Dispatchable virtual oscillator control for decentralized inverter-dominated power systems: Analysis and experiments. In *2019 IEEE Applied Power Electronics Conference and Exposition (APEC)*, pages 561–566, 2019.
- [11] N. Cohn. *Control of Generation and Power Flow on Interconnected Power Systems*. J. Wiley, 1966.
- [12] Stefanos Baros, Yu Christine Chen, and Sairaj V. Dhople. Examining the economic optimality of automatic generation control. *IEEE Transactions on Power Systems*, 36(5):4611–4620, 2021.
- [13] John W. Simpson-Porco. On area control errors, area injection errors, and textbook automatic generation control. *IEEE Transactions on Power Systems*, 36(1):557–560, 2021.
- [14] Olaoluwapo Ajala, Minghui Lu, Brian Johnson, Sairaj V. Dhople, and Alejandro Domínguez-García. Model reduction for inverters with current limiting and dispatchable virtual oscillator control. *IEEE Transactions on Energy Conversion*, 37(4):2250–2259, 2022.
- [15] Manish Singh, D. Venkatramanan, and Sairaj Dhople. Towards optimal primary- and secondary-control design for networks with generators and inverters. In *Proc. Allerton Conference on Communication, Control, and Computing*, pages 1–6, 2022.
- [16] D. Venkatramanan and Sairaj Dhople. Per-unit modeling via similarity transformation. *IEEE Transactions on Energy Conversion*, 38(2):825–837, 2023.
- [17] L. Ljung. *System identification toolbox: User's guide*. Citeseer, 1995.

Appendix A

Glossary and Acronyms

A.1 Glossary

- **Automatic generation control (AGC)** – A secondary control layer on the power grid, responsible for returning the frequency within a single area to nominal while matching power demand.
- **Economic dispatch** – A tertiary control layer on the power grid, responsible for finding the optimal power generation mix in order to minimize cost while meeting load.
- **IEEE 14-bus network** – A standard test case for power control algorithms; approximates a portion of the American power grid as of February 1962.
- **Inverter-based resource (IBR)** – A power source interfaced to the grid via a DC-AC inverter.
- **Grid-following inverter (GFL)** – An inverter-based resource that synchronizes its frequency to that provided by the external grid.
- **Grid-forming inverter (GFM)** – An inverter-based resource that is capable of setting its frequency independent of the external grid.
- **System identification** – A set of mathematical techniques for discovering the internal dynamics of an existing system.

- **System identification toolbox (SIT)** – The library built into Matlab for performing system identification.

A.2 Acronyms

Table A.1: List of acronyms used in this paper

Acronym	Meaning
AGC	Automatic generation control
CCVS	Current-controlled voltage source
dVOC	Dispatchable virtual oscillator
IBR	Inverter-based resource
GFL	Grid-following inverter
GFM	Grid-forming inverter
SIT	System identification toolbox
SSM	Simplified synchronous machine
VSM	Virtual synchronous machine